J. Opt. B: Quantum Semiclass. Opt. **2** (2000) 633–644. Printed in the UK PII: S1464-4266(00)10402-1

Quantum transport in magneto-optical double-potential wells

Ivan H Deutsch†, Paul M Alsing†, John Grondalski†, Shohini Ghose†, David L Haycock‡ and Poul S Jessen‡

† Department of Physics and Astronomy, Center for Advanced Studies, University of New Mexico, Albuquerque, NM 87131, USA
‡ Optical Sciences Center, University of Arizona, Tucson, AZ 85721, USA

Received 15 December 1999, in final form 4 May 2000

Abstract. We review the quantum transport of ultra-cold alkali atoms trapped in a one-dimensional optical lattice of double-potential wells, engineered through a combination of ac-Stark shifts and Zeeman interactions. The system is modelled numerically through analysis of the bandstructure and integration of the time-dependent Schrödinger equation. By these means we simulate coherent control of the atomic wavepackets. We present results from ongoing experiments on laser-cooled caesium, including the demonstration of quantum state preparation and preliminary evidence for coherent tunnelling. Entanglement between the internal and motional degrees of freedom allows us to access the tunnelling dynamics by Stern–Gerlach measurements of the ground state magnetic populations. A scheme to extend this into a full reconstruction of the density matrix for the ground state angular momentum is presented. We further consider the classical dynamics of our system, which displays deterministic chaos. This has important implications for the distinction between classical and quantum mechanical transport.

Keywords: Quantum tunelling, chaos, optical lattices

1. Introduction

Dynamics associated with a particle in a double-potential well play a key role in numerous areas of pure and applied sciences, and is an important paradigm for quantum coherent evolution. Most fundamental is the decay or oscillation of a meta-stable state via quantum tunnelling. For example, in chemical kinetics, 'reactants' and 'products' experience potential well minima with an activation barrier U_B between them. Quantum tunnelling plays a role at low temperatures in modifying the usual Arrhenius law for the transition rate $\Gamma = \nu_0 \exp[-U_B/k_B T]$ [1]. Familiar examples of quantum tunnelling in double wells are numerous in other physical systems. Examples for condensed matter include electron transport in semiconductor quantum wells [2], quasiparticle transport in the molecular polaron model [3], and defect tunnelling in crystals and amorphous solids which influences their dielectric and acoustic properties [4].

Of particular interest is the tunnelling of meso/macroscopic degrees of freedom [5]. Examples include tunnelling of Cooper pairs through a Josephson junction [6], and the tunnelling of the total cooperative magnetization (or Néel) vector in ferromagnetic (or anti-ferromagnetic) grains with anisotropic magnetic fields, as proposed by Chudnovsky and Tejada [7]. In many of these systems, coupling to the noisy environment leads to dissipation which strongly influences the tunnelling dynamics. There is a wealth of literature on the role of dissipation in tunnelling, stimulated by the seminal work of Caldeira and Leggett [5, 8]. An important question is the effect of dissipation on the phase transition between coherent quantum transport and thermal hopping [9]. Besides its importance for the performance of devices such as SQUIDS [6] and tunnelling microscopes [10], this problem is of fundamental interest in the study of macroscopic quantum coherence and the boundary between quantum and classical dynamics [11]. The decay of macroscopic superposition states via environment-induced decoherence is central to our current understanding of the emergent classical behaviour [12]. Tunnelling over macroscopic distances result in delocalized states which are extremely susceptible to decoherence, and it remains a key challenge to design systems in which the regime of quantum coherent dynamics, as well as the gradual transition to classical dynamics, can be experimentally accessed.

The control of dissipation in quantum coherent systems is increasingly important for new applications in quantum information processing, such as quantum computing [13]. In one proposal, quantum logic would be implemented via spin-dependent quantum tunnelling between coupled single-electron quantum dots [14]. Suppression of decoherence is crucial to the performance of such a device. In this context there has been great interest in controlling

dissipative tunnelling dynamics through the application of coherent driving forces [15]. Phenomena such as dynamic localization [16] and stochastic resonances [17] arise through the interplay between quantum interference, coherent drives and noise.

Another fundamental problem in the quantum–classical transition is the emergence of chaos in a nonlinear system. One paradigm for such studies is the driven double well [18]. By monitoring the quasiprobability distribution in phase space, one finds that localized regions of phase space, corresponding to classically stable regions bounded by KAM (Kolmogorov–Arnol'd–Moser) surfaces, are now connected by quantum tunnelling. The transition rate between these stable islands can be much greater than the ordinary tunnelling rate, a phenomenon known as 'chaos assisted tunnelling' [19].

We consider here the dynamics of ultra-cold atoms in magneto-optical potentials as an ideal system in which to explore the wide variety of phenomena associated with double-potential wells. Optical lattices, arising from the ac-Stark effect associated with a set of interfering laser beams [20], have proven to be a very clean system to investigate quantum transport phenomena, including Bloch oscillations [21], Wannier–Stark ladders [22], Landau–Zener tunnelling [23], dynamical band-collapse [24], and tunnelling in gauge potentials [25]. The properties which make this system well suited to this research are discussed throughout this issue:

- The optical potential can be made nondissipative in the far-off resonance limit.
- Pure quantum states can be prepared through cooling [26] and state selection techniques [23], and their subsequent evolution and decoherence monitored by measuring the density matrix for the atomic internal state [27].
- Properties of the lattice can be dynamically varied through changes in the laser parameters such as intensity, frequency, wavevector direction, polarization, and through the addition of external magnetic and/or electric fields.
- Noise can be reintroduced into the system in a well characterized way [28].

Coherent control of atomic wavepackets can be achieved in optical lattices [29] in a manner similar to that performed in ion traps [30], with a flexibility reflected in the rich atom–field interaction. This flexibility will allow us to study the interplay of quantum dynamics, classical instabilities, coherent and stochastic external driving fields, and quantum noise.

The remainder of this paper is organized as follows. In section 2 we review the theoretical model for the system under consideration—a far-off resonance optical lattice trapping alkali atoms such as caesium, together with external magnetic fields. Through an appropriate choice of geometry, the magneto-optical potential consists of a lattice of double-potential wells with variable barrier height, energy asymmetry and separation. We describe our Hamiltonian and solution methods, including numerical simulations of the time-dependent Schrödinger equation for our hyperfine-spinor wavepacket. In section 3 we detail our experimental setup and measurements. A particularly appealing aspect of quantum transport studies in optical potentials is that we can bring to bear the full plethora of quantum control techniques: pure state preparation, controlled unitary evolution and quantum state readout. Coherent tunnelling is directly observable from a measurement of time-varying microscopic quantities, such as the populations of atomic magnetic sublevels, rather than through an indirect signature in the macroscopic properties of an ensemble in thermodynamic equilibrium, as is often the case in condensed-matter systems. Section 4 discusses further phenomena which we are currently exploring, both theoretically and experimentally. In order to fully characterize the coherent dynamics of our system one must implement quantum state measurement techniques which measure the off-diagonal matrix elements of the density operator [27]. We describe a scheme to reconstruct the ground state angular momentum density matrix for our spinor wavepacket [31], and show the result of a numerical simulation to demonstrate its robustness. We end this section with a discussion of the classical dynamics associated with motion of the atoms in the magneto-optical double-potential well. Such an analysis is necessary to identify those aspects of the transport which are uniquely quantum mechanical. This is especially important for our system where the Born–Oppenheimer approximation (BOA) breaks down, and one can no longer treat the dynamics as occurring on an effective one-dimensional potential surface. Instead the effective phase space is multidimensional, and the total energy does not uniquely determine the classical path and can even be chaotic. Our system can be mapped onto the Jaynes–Cummings [32] (or generally Tavis–Cummings [33]) Hamiltonian, without the rotating wave approximation, which is known to exhibit classical chaos [34]. Finally, in section 5 we summarize our results.

2. Theoretical model

2.1. Optical lattices—the effective magnetic field picture

We consider an optical lattice formed by a monochromatic field with arbitrary polarization, $\boldsymbol{E}(\boldsymbol{x},t) = \mathrm{Re}\,(\boldsymbol{E}(\boldsymbol{x})\mathrm{e}^{-\mathrm{i}\omega_L t})$. The light-shift potential has the form [20]

$$\hat{U}_{\mathrm{LS}}(\boldsymbol{x}) = -\tfrac{1}{4}\boldsymbol{E}^*(\boldsymbol{x})\cdot\hat{\overleftrightarrow{\alpha}}\cdot\boldsymbol{E}(\boldsymbol{x}), \tag{1}$$

where $\hat{\overleftrightarrow{\alpha}} = -\sum_e \hat{\boldsymbol{d}}_{ge}\hat{\boldsymbol{d}}_{eg}/\hbar\Delta_{eg}$ is the atomic polarizability tensor for the optical transition $|g\rangle \to |e\rangle$, with $\hat{\boldsymbol{d}}_{eg}$ the dipole operator and $\Delta_{eg} = \omega_L - \omega_{eg}$ the detuning. Decomposing these tensors into their irreducible components,

$$\hat{U}_{\mathrm{LS}}(\boldsymbol{x}) = -\tfrac{1}{4}\left(|\boldsymbol{E}(\boldsymbol{x})|^2\hat{\alpha}^{(0)} + (\boldsymbol{E}^*(\boldsymbol{x})\times\boldsymbol{E}(\boldsymbol{x}))_i\hat{\alpha}_i^{(1)} + \left(\frac{E_i^*E_j + E_j^*E_i}{2}\right)\hat{\alpha}_{ij}^{(2)}\right), \tag{2a}$$

$$\hat{\alpha}^{(0)} = \sum_e \tfrac{1}{3}\hat{\boldsymbol{d}}_{ge}\cdot\hat{\boldsymbol{d}}_{eg}, \qquad \hat{\alpha}_i^{(1)} = \sum_e \varepsilon_{ijk}\hat{\boldsymbol{d}}_{ge}^j\hat{\boldsymbol{d}}_{eg}^k,$$
$$\hat{\alpha}_{ij}^{(2)} = \sum_e \tfrac{1}{2}(\hat{\boldsymbol{d}}_{ge}^i\hat{\boldsymbol{d}}_{eg}^j + \hat{\boldsymbol{d}}_{ge}^j\hat{\boldsymbol{d}}_{eg}^i) - \hat{\alpha}^{(0)}\delta_{ij}. \tag{2b}$$

Thus, by appropriate choice of atomic transition and field distribution, we can design scalar, vector and tensor interactions.

We restrict our attention here to alkali atoms excited on the so-called D2 resonance, $|S_{1/2}\rangle \rightarrow |P_{3/2}\rangle$. When the detuning is sufficiently large (but still small compared with the fine structure splitting), hyperfine splitting can be neglected and the ground state polarizability is essentially that of a $|J = \frac{1}{2}\rangle$ atom. In that case the rank-2 tensor interaction vanishes and only scalar and vector interactions are possible. This is in strong contrast to the situation in which the atom is excited close to one of the excited hyperfine states. In that case strong tensor couplings occur as well. The resulting optical potential in the far-off resonance limit then has the form of a scalar plus Zeeman-like interaction with a fictitious magnetic field [35],

$$\hat{U}_{\rm LS}(\boldsymbol{x}) = U_0(\boldsymbol{x}) - \hat{\vec{\mu}} \cdot \boldsymbol{B}_{\rm fict}(\boldsymbol{x}). \tag{3}$$

We assume the atoms are optically pumped into a given hyperfine ground state with quantum number F and magnetic moment $\hat{\vec{\mu}} = \hbar\gamma\hat{\boldsymbol{F}}$, where $\hat{\boldsymbol{F}}$ is the vector angular momentum operator for this state and $\gamma = -g_F\mu_B/\hbar$ is the gyromagnetic ratio. If we further assume that our field is a superposition of plane waves of amplitude E_1, and write $\boldsymbol{E}(x) = E_1\vec{\varepsilon}_L(x)$, we find [29],

$$\begin{aligned} U_0(\boldsymbol{x}) &= \tfrac{2}{3}U_1(\vec{\varepsilon}_L^*(\boldsymbol{x}) \cdot \vec{\varepsilon}_L(\boldsymbol{x})), \\ \mu_B\boldsymbol{B}_{\rm fict}(\boldsymbol{x}) &= \frac{1}{3}U_1\left(\frac{\vec{\varepsilon}^*(\boldsymbol{x}) \times \vec{\varepsilon}(\boldsymbol{x})}{\mathrm{i}}\right). \end{aligned} \tag{4}$$

Here U_1 is the light shift produced by a single lattice beam (<0 for red detuning) driving a transition with unit oscillator strength. To set the scales, for caesium with $F = 4$, $g_F\mu_B = 0.17E_{\rm R}$ mG^{-1}, where $E_{\rm R} = (\hbar k_L)^2/(2M) \approx h(2\,\mathrm{kHz})$ is the photon-recoil energy.

The above optical potential, together with real magnetic fields $\boldsymbol{B}$, can be used to design lattices of double-potential wells. In the lin-θ-lin configuration [36] consisting of counterpropagating plane waves with linear polarizations at an angle θ (see figure 1(*a*)), we have $\vec{\varepsilon}_L(z) = \boldsymbol{e}_x\mathrm{e}^{\mathrm{i}k_Lz} + (\boldsymbol{e}_x\cos\theta + \boldsymbol{e}_y\sin\theta)\mathrm{e}^{-\mathrm{i}k_Lz}$, giving

$$\begin{aligned} \hat{U}(z) = {} & \tfrac{2}{3}U_1\{(2 + 2\cos\theta\cos(2k_Lz)) \\ & - (\sin\theta\sin(2k_Lz))\hat{F}_z/F\} - \hbar\gamma\hat{\boldsymbol{F}} \cdot \boldsymbol{B} \\ = {} & \tfrac{4}{3}U_1 + \sum_m U_m\cos(2k_Lz + \phi_m)|F, m\rangle\langle F, m| \\ & - \hbar\gamma\hat{\boldsymbol{F}} \cdot \boldsymbol{B}, \end{aligned} \tag{5}$$

where

$$U_m = \frac{2}{3}U_1\sqrt{4\cos^2\theta + \left(\frac{m}{F}\right)^2\sin^2\theta}$$

and $$\tan\phi_m = \frac{m}{2F}\tan\theta.$$

The optical potential is diagonal in the basis of magnetic sublevels quantized along z (off-diagonal elements vanish in the far-off resonance limit as described above). Each 'diabatic potential' then represents a simple sinusoid of different amplitude and phase. These potentials cross at positions of linear polarization where the fictitious magnetic field of equations (3), (4*b*) vanish (see figure 1(*b*)). A real magnetic field along the quantization axis gives rise to a uniform Zeeman shift, but does not induce coherence between these levels. A real magnetic field transverse to the quantization axis breaks the degeneracy. The resulting *adiabatic* potential exhibits a lattice of *double-potential wells* (figures 1(*c*) and (*d*)) for the lowest few potential curves.

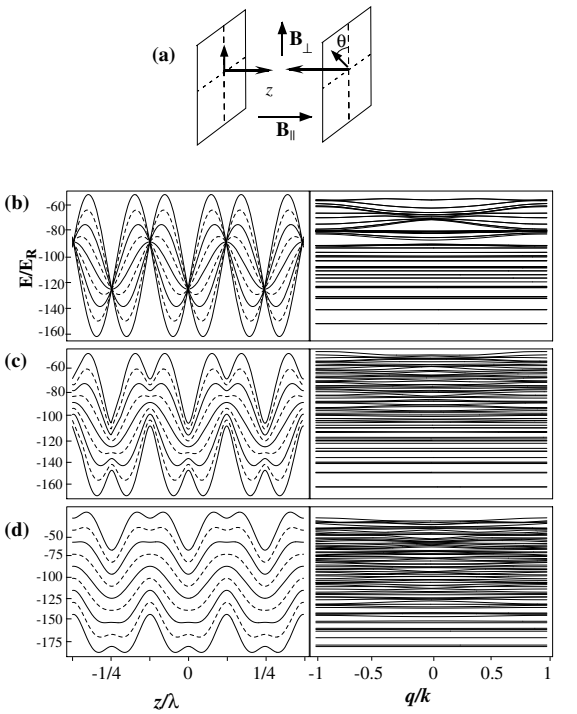

Figure 1. Magneto-optic potentials for the hyperfine ground state $F = 4$ in the far-off resonance limit. (*a*) Counterpropagating lattice beams create $\sigma+$ and $\sigma-$ polarized standing waves along z, with a relative spatial phase determined by the angle θ formed by the linear polarizations, producing sinusoidal potentials for each magnetic sublevel. An axial magnetic field $\boldsymbol{B}_\parallel$ provides a dc-bias of each potential and a transverse magnetic field $\boldsymbol{B}_\perp$ couples them pairwise. The resulting nine adiabatic potentials and energy bands in the first Brillouin zone are shown in (*b*)–(*d*) for $U_1 = -83E_{\rm R}$, $\theta = 80^\circ$, $\boldsymbol{B}_\parallel = 0$ mG and: (*b*) $\boldsymbol{B}_\perp = 0$ mG (no coupling), (*c*) $\boldsymbol{B}_\perp = 30$ mG (weak coupling), (*d*) $\boldsymbol{B}_\perp = 85$ mG (moderate coupling). Anticrossings in the lowest potentials exhibit a double-well at each $\lambda/4$ lattice site. Negligible band curvature for lowest bands indicate negligible site-to-site tunnelling. The transverse magnetic fields split previously degenerate ground-bands in (*b*) into a doublet with $\Delta E = 8.5 \times 10^{-2}E_{\rm R}$ and $\Delta E = 1.8E_{\rm R}$ for (*c*) and (*d*) respectively.

An atom initially trapped with very low energy at one of the lattice sites experiences the dynamics of the double wells; tunnelling between different double wells at *different sites* separated by $\lambda/4$ is strongly suppressed by the large energy barrier separating them and can be neglected over the timescale of the on-site dynamics. In that case one can use a harmonic expansion around the minima. Adding a true external magnetic field with free-space Lamor frequency $\vec{\Omega}_L = \gamma\boldsymbol{B}$, the potential in the basis of magnetic sublevels has the approximate form,

$$\hat{U} = \sum_m \tfrac{1}{2}M\omega_m^2(\hat{z} + \Delta z_m/2)^2|m\rangle\langle m| - \hbar\vec{\Omega}_L \cdot \hat{\boldsymbol{F}}, \tag{6a}$$

where

$$\hbar\omega_m = 2\sqrt{2|U_m|E_R}, \qquad \Delta z_m = \lambda_L \frac{\phi_m}{2\pi}. \tag{6b}$$

For the special case of spin-$\frac{1}{2}$ ($F = \frac{1}{2}$), the Hamiltonian reduces to a familiar expression,

$$\hat{H} = \left(\frac{\hat{p}^2}{2M} + \frac{1}{2}M\omega^2\hat{z}^2\right) - \frac{\hbar\Omega_x}{2}\hat{\sigma}_x + \left(\frac{1}{2}M\omega^2\Delta z\hat{z} - \frac{\hbar\Omega_z}{2}\right)\hat{\sigma}_z, \tag{7}$$

where $\omega = \omega_{m=F}$, and we have neglected a constant term. This system, consisting of a single-mode harmonic oscillator coupled to a spin-$\frac{1}{2}$ particle, is known alternately in the condensed matter community as the 'spin–boson' problem [8] and in the quantum optics community as the 'Jaynes–Cummings' problem [32]. We will return to this model in section 4.2.

It is useful to view these potentials in terms of total effective magnetic field—fictitious plus real field. Because the atomic position is correlated with the internal state (through the effective magnetic field), precession of the atomic spin about the external B-field is accompanied by motion of the atomic centre-of-mass wavepacket. Our problem thus has a kinship with the mesoscopic magnetization problem of Chudnovsky [7] discussed in the introduction. In contrast to the condensed matter problem, here the oscillation of the atomic magnetization is correlated with centre-of-mass motion over mesoscopic distances. The oscillation of magnetization provides a meter through which we can detect the time-dependent motion of the packet.

2.2. Solutions to the Schrödinger equation

2.2.1. Band structure. We calculate the energy bandstructure numerically, starting from the Hamiltonian with the potential given in equation (5). The eigenstates are Bloch spinors, $|\Psi_{n,q}\rangle = \sum_m e^{iqz}|u^{(m)}_{n,q}\rangle \otimes |m\rangle$, where $|u^{(m)}_{n,q}\rangle$ is the periodic wavefunction for magnetic sublevel m, and q is the quasimomentum [20]. For sufficiently deep wells, the lower bands show no appreciable curvature, indicating negligible site-to-site tunnelling (see figures 1(*b*)–(*d*)). It is then appropriate to treat the state at a given lattice site as a local Wannier-spinor [37], with a harmonic oscillator-like wavefunction for each component. Without a transverse magnetic field, the Hamiltonian is diagonal in the magnetic substate basis and the eigenstates are doubly degenerate, corresponding to an anti-ferromagnetic symmetry. In the presence of a finite transverse magnetic field $\boldsymbol{B}_\perp$ the axial-rotation symmetry is broken and all magnetic substates are coupled. The resulting eigenstates satisfy the combined symmetry of parity together with a spin-flip, $u^{(m)}_n(z) = \pm u^{(-m)}_n(-z)$ [29]. The ground band is split, with an energy difference that gives a 'tunnelling frequency' Ω_T on the order of $\Omega_\perp|\langle\psi_L|\psi_R\rangle|$, where $\Omega_\perp = \gamma\boldsymbol{B}_\perp$ is the bare Larmor precession frequency of the transverse field and $|\langle\psi_L|\psi_R\rangle|$ measures the overlap between the wavefunctions localized in the left and right wells.

In viewing the bandstructure one should not associate a given energy band with a single adiabatic potential curve. Indeed, the ground band doublet in figure 1(*d*) appears *above* the barrier of the lowest adiabatic potential, where one might have expected no doublet at all. This feature reflects that fact that the BOA, which holds when the internal state evolves much more rapidily than the external motional states, breaks down for this system (see Dutta and Raithel in this issue). Thus, though the adiabatic potentials give us an indication of how the different internal states are coupled as a function of position, they *do not* give us a picture of the classical force exerted on our atoms. As a consequence, the distinction between classical and quantum transport in this system cannot be immediately gleaned from these potential curves, and one must resort to a more sophisticated analysis. We will return to this interpretational issue in section 4.2 after consideration of the preliminary experimental results.

2.2.2. Numerical simulation. The bandstructure contains some quantitative information about the dynamical timescales associated with atomic motion in the magneto-optic potential. However, one must ultimately solve the time-dependent Schrödinger equation to fully explore the possibilities for quantum state preparation and control. We thus turn to numerical techniques. Simulation of wavepacket motion in complex potentials has been the subject of a recent study, especially in the context of atomic collisions and quantum chemistry [38]. Our problem has the interesting and complicating feature of the entanglement between internal and external degrees of freedom.

The propagator of the $2F+1$ spinor state, $|\psi(t+\Delta t)\rangle = \hat{U}(\Delta t; t)|\psi(t)\rangle$, can be approximated for small time steps by a split step operator procedure, which for a Hamiltonian $\hat{H}(t) = \hat{T} + \hat{V}(t)$ [39] has the form

$$\hat{U}(\Delta t; t) \approx e^{-\frac{i}{\hbar}\hat{H}(t)\Delta t} \approx e^{-\frac{i}{\hbar}\frac{\hat{T}}{2}\Delta t}e^{-\frac{i}{\hbar}\hat{V}(t)\Delta t}e^{-\frac{i}{\hbar}\frac{\hat{T}}{2}\Delta t}. \tag{8}$$

This method is accurate through to order $(\Delta t)^2$ and robust because the propagator is norm preserving. Typically, one uses a fast Fourier transform to efficiently translate between position and momentum representations, where respectively the kinetic and potential energy are usually diagonal. The potential of equation (5), however, is not diagonal in the position representation when a transverse magnetic field is present, but rather tri-diagonal. This requires a computationally intensive matrix exponentiation at every time step when the potential varies as a function of t. A better way to factorize the small time propagator is to write the exponentials in their Cayley form, which is also second-order accurate and unitary [40],

$$\hat{U}(\Delta t; t) \approx \left(\frac{1 - \frac{i}{4}\hat{T}\Delta t}{1 + \frac{i}{4}\hat{T}\Delta t}\right) \times \left(\frac{1 - \frac{i}{2}\hat{V}(t)\Delta t}{1 + \frac{i}{2}\hat{V}(t)\Delta t}\right)\left(\frac{1 - \frac{i}{4}\hat{T}\Delta t}{1 + \frac{i}{4}\hat{T}\Delta t}\right). \tag{9}$$

The computationally intensive operation at each time step now involves an inversion of a tri-diagonal matrix for which efficient algorithms exist [41].

The first simulations we perform show that a spinor wavepacket, initially in the ground state, can be mapped through an appropriate dynamic application of magnetic

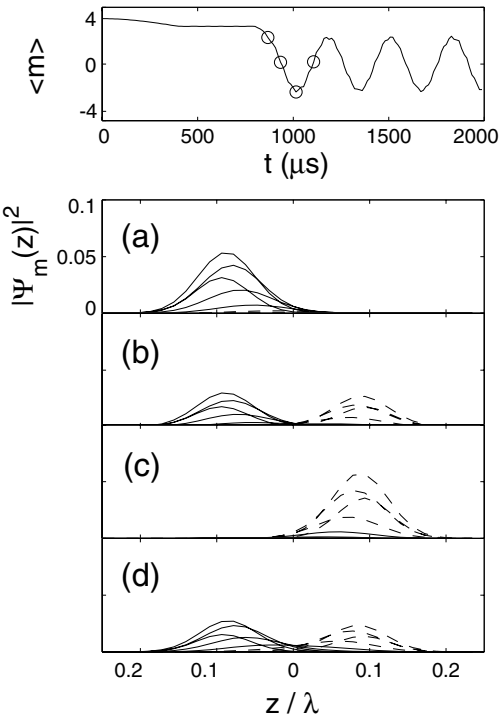

Figure 2. Numerical simulation of quantum state preparation leading to magnetization oscillation and quantum tunnelling. The lin-θ-lin lattice is constructed with $\theta = 81^\circ$ and single-beam light-shift $|U_1| = 81E_R$. An initial bias field of $B_z = -55$ mG maintains the atom in the pure $m = 4$ state. A transverse magnetic field is ramped to $B_x = 85$ mG in 400 μs. After coherences are established, the bias field is ramped to zero in 77 μs, mapping the initial state onto a superposition of the ground band doublet. Evolution of the average magnetization is plotted during this procedure. The absolute square of the nine components of the spinor wavepacket are plotted at different snap shots of the tunnelling oscillation (*a*)–(*d*), with negative *m*-states dashed.

fields onto a two-dimensional Hilbert space associated with a tunnelling wavepacket. As detailed further in section 3 below, atoms are at some point in time prepared in the ground state of the lowest potential of a lattice with a large axial field B_z. We then apply a transverse field B_x and ramp the axial field to zero, in order to produce an initially localized state in a symmetric double-potential well. Because the energy eigenstates are now the symmetric and anti-symmetric states, an initially localized atom will tunnel at a frequency given by the ground band energy splitting. An implicit assumption in this procedure is that there is a clean separation between timescales. The turn-off of B_z must be fast compared with the ground-band frequency splitting, so as to avoid adiabatic transformation of the wavepacket into the symmetric state, but slow compared with the energy difference between the doublet and the excited states, so as to avoid populating higher lying energy bands. In practice this condition is easily met over a wide range of parameters. In figure 2 we show the result of simulations of this procedure to create tunnelling wave packets. Strong magnetization oscillations at the tunnelling frequency are seen together with a time sequence of the wavepacket spinors associated with these oscillations.

3. Experiment

3.1. The one-dimensional lin-θ-lin lattice

We have recently performed a series of experiments to demonstrate the potential for systematic studies of quantum tunnelling in double-well optical lattices of the type given in equation (5). Our setup consists of a pair of counterpropagating laser beams with linear polarizations forming a fixed but adjustable angle θ (see figure 3(*a*)). To provide for time-of-flight analysis of the atomic momentum distribution, the lattice axis (defined by the beam directions) is vertical to within a few mRad. The lattice beams are derived from a single 0.5 W master oscillator–power amplifier (MOPA) diode laser system detuned 16 GHz ($\sim$3000 Γ) below the $6S_{1/2}(F = 4) \leftrightarrow 6P_{3/2}(F' = 5)$ laser-cooling transition in caesium. The intensities and frequencies of the two beams are independently controlled by acousto-optic deflectors, whose driving frequencies are synthesized from a single quartz oscillator. This provides accurate, programmable control of the lattice depth and acceleration in the laboratory frame. The external magnetic fields B_x and B_z are applied by magnet coils controlled by arbitrary waveform generators. As described in the following, this allows us to prepare an initial pure state and to coherently manipulate the tunnelling process through full computer control of the magneto-optic potential.

Quantum tunnelling is exponentially sensitive to the double-well barrier, and a well-controlled experiment therefore requires considerable care in reproducing the potential of equation (5). The laser beams used to create the lattice must have uniform intensity so that the single-beam light shift U_1 does not vary across the atomic sample. We inspect each of the beams independently with a CCD camera and verify that their intensity profiles are homogeneous to within roughly 5% RMS. A more difficult problem is the elimination of spurious magnetic fields, both in the form of ambient real fields and in the form of spurious fictitious fields (equation (4)) caused by elliptic lattice beam polarizations. We cancel the ambient real magnetic field across the entire volume occupied by the atomic sample, by applying a compensating field with controlled gradients. By measuring the Larmor precession rate and dephasing of the magnetic moments, we estimate that the average value of the remnant real field is typically less than $\sim\frac{1}{4}$ mG, with a homogeneity of $\sim$10 μG across the atomic sample. Controlling and minimizing the spurious fictitious field is more challenging. We use high-quality Glan-laser-type calcite polarizers (crossed-polarizer extinction $\leqslant 10^{-6}$) to define the linear beam polarizations, but birefringence in the vacuum windows and the lower fold mirror (see figure 3(*a*)) will potentially introduce ellipticity, and hence a spurious fictitious B_z. In the one-dimensional lin-θ-lin geometry the combined polarization errors of the interfering lattice beams thus results in an energy asymmetry of the double wells. The corresponding asymmetry of the tunnelling oscillations can be observed and cancelled with a compensating real field. By symmetrizing the tunnelling oscillations we are able to cancel all spurious fields (real and fictitious) to better than $\sim$1 mG. Residual polarization errors which are not uniform across the lattice beams are most likely the dominant source

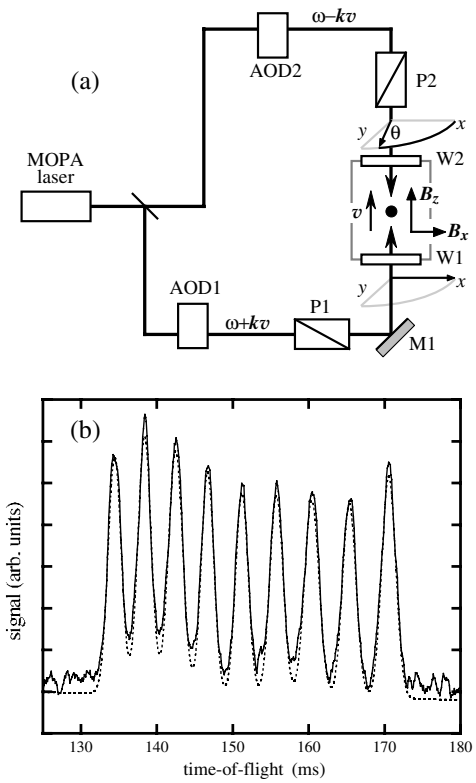

Figure 3. (*a*) Optical part of the double-well optical lattice setup. Both lattice beams originate from a single MOPA source, with intensity and frequency independently controlled by acousto-optic deflectors AOD1 and AOD2. A frequency difference of $2kv$ moves the lattice at velocity v in the laboratory frame, and provides computer control of the lattice acceleration. Polarizers P1 and P2 define the beam polarizations and the angle θ between them. Polarization purity at the atomic sample is limited by residual birefringence in the fold mirror M1 and the vacuum windows W1 and W2. (*b*) Stern–Gerlach measurement showing the nine resolved time-of-flight distributions for the states $-4 \leqslant m \leqslant 4$ in the $F = 4$ hyperfine ground state of Cs. For the purpose of illustration the magnetic sublevels were nearly uniformly populated by Larmor precession in a noisy magnetic field. The dotted curve is a fit to a sum of nine Gaussians.

of inhomogeneous broadening of the tunnelling resonance, and result in dephasing of the tunnelling oscillations.

3.2. Quantum state preparation

At the beginning of a tunnelling experiment we prepare atoms in the lattice in a pure quantum state localized on, e.g., the left side ($z < 0$) of the optical double-well potential. This quantum state preparation is accomplished via a series of steps that include laser cooling, optical pumping, and state selection and manipulation in the lattice. Laser cooling begins with a standard MOT/3D optical molasses setup, which prepares a cold sample of $\sim 10^6$ Cs atoms with a temperature of $\sim 4\ \mu$K and a Gaussian density distribution of $\sim 200\ \mu$m RMS radius. The atoms are then transferred to a near-resonance one-dimensional lin-θ-lin lattice tuned $\sim 17\,\Gamma$ below the $6S_{1/2}(F = 4) \leftrightarrow 6P_{3/2}(F' = 5)$ transition for a second cooling stage. During this time a small magnetic field is applied in order to maximize the population accumulated in the lowest vibrational state of the lattice potential associated with the $m = 4$ magnetic sublevel [42]. After 1.5 ms of one-dimensional cooling the atoms are adiabatically transferred to the far-off-resonance double-well lattice [43] where they are optically pumped to the $m = 4$ potential. Next we decrease the lattice depth to a point where only the lowest energy band is bound and accelerate the lattice at 300 m s^{-2} for 1.5 ms. At the same time we apply a field $B_z = -55$ mG, large enough to lift all degeneracies between potentials for different m and confine the centre-of-mass dynamics to the $m = 4$ potential. During the acceleration phase, atoms in the ground band remain trapped in the potential wells of the moving lattice and acquire a total upward velocity of 0.45 m s^{-1}, while atoms in higher bands are not trapped and undergo no significant change in velocity. At later times these two groups of atoms follow different ballistic trajectories and give rise to two clearly separated distributions in a time-of-flight spectrum. Therefore, if we look only at the distribution corresponding to atoms that follow the lattice during accelleration, we have effectively prepared a sample in the ground vibrational state of the (isolated) potential wells of the $m = 4$ potential [23]. Based on a subsequent measurement of the momentum distribution and the populations of the magnetic sublevels we estimate that our state selection procedure prepares atoms with $\sim$90% population in this target state. When the state selection is completed we increase the lattice depth to the value used for the tunnelling experiment, and change the accelleration so the lattice frame is in free fall. Finally, to initiate tunnelling oscillations we evolve the ground state of the $m = 4$ potential into a localized state in the double-potential well, as detailed in section 2.2.2 above. In the experiment this is accomplished by first ramping B_x from zero to the desired value in 250 ms, and then ramping B_z to zero in 70 ms. Our simulations confirm that this sequence transforms the atomic spinor wavepacket as desired.

3.3. Zeeman microscope

A unique aspect of our magneto-optical double-well system is the possibility to use the atomic internal state as a 'meter' to detect tunnelling. The left/right-localized states in the double-well potential are Wannier spinors, i.e., localized wavepackets which are entangled states of internal and external degrees of freedom. Information about the motional degrees of freedom can therefore be obtained through a measurement of the magnetic populations, a technique we have nicknamed the 'Zeeman microscope'. If the light field on the left (right) sides of the barrier is predominantly $\sigma_+(\sigma_-)$ polarized, then the localized states have predominantly $m > 0 (m < 0)$ character. A similar correlation between position and internal state has been used to observe atom transport in optical gauge potentials, based on photon redistribution between the lattice beams as atoms tunnelled between σ_+ and σ_- sites [25].

To observe tunnelling we track the evolution of the atomic internal state by Stern–Gerlach measurements of the atomic populations at different times. This approach is particularly suitable for laser-cooled atoms, since the narrow momentum distribution permits us to resolve the magnetic sublevels of large angular momenta ($F = 4$ in the case of caesium) with modest magnetic field gradients. Our Stern–Gerlach measurement is performed with a straightforward

modification of the standard time-of-flight technique [44]. As atoms are released from the lattice and fall under the influence of gravity to a probe beam located a few cm below the lattice volume, we apply a magnetic field gradient of $\sim$13 G cm^{-1} for a period of 35 ms. The actions of the resulting forces $F_m = -g_F\mu_B\nabla|\boldsymbol{B}| \cdot m$ are sufficiently different to completely separate the time-of-flight distributions for different m. An example is given in figure 3(b), which shows nine distinct peaks corresponding to the values $-4 \leqslant m \leqslant 4$ for the $F = 4$ ground state of Cs. Variations in the detection efficiency for different m occur because some atoms follow trajectories that miss the probe beam, and because atoms in different states pass through the probe beam with different velocity. These effects are easily modelled and accounted for, and fits to the separate time-of-flight distributions can be used to obtain accurate measures for the populations and temperatures of different m. We have previously used this technique to study laser cooling in optical lattices [26, 42].

3.4. Coherent dynamics

We have successfully used the Zeeman microscope technique to observe coherent tunnelling in an optical double-well potential. Initially we prepare the left-localized state in a lattice with $U_1 \approx 83E_{\mathrm{R}}$ and $\theta = 80^\circ$ as described above. This state subsequently undergoes tunnelling oscillations at a frequency given by the splitting of the ground band doublet. For a typical $B_x = 85$ mG we compute the bandstructure of figure 4(a), which predicts a tunnelling oscillation frequency $\Omega_T \approx 1.7E_{\mathrm{R}} \approx 3600$ Hz and period $\tau_T \approx 280$ μs. Based on our simulations we expect that that the dynamics can, to a good approximation, be restricted to the ground band doublet. In that case the time-dependent tunnelling state is approximately $|\psi(t)\rangle = (|\psi_S\rangle + \mathrm{e}^{-\mathrm{i}\Omega_T t}|\psi_A\rangle)/\sqrt{2}$, where $|\psi_S\rangle$, $|\psi_A\rangle$, are the symmetric/antisymmetric Wannier spinors corresponding to the ground doublet.

Figure 4(c) shows experimental measurements of the magnetic populations as the atoms oscillate from a left-localized state to a right-localized state and back, with some loss of contrast. Under the two-level assumption the best fit to the observed magnetization correspond to a $\sim$98% population of $|\psi_L\rangle$ at $t \approx 0$, $\sim$77% population of $|\psi_{\mathrm{R}}\rangle$ at $t \approx \tau_T/2$ and $\sim$56% population of $|\psi_L\rangle$ at $t \approx \tau_T$. At $t \approx \frac{1}{4}\tau_T$ oscillation period the distribution is consistent with a delocalized state $(|\psi_S\rangle - \mathrm{i}|\psi_A\rangle)/\sqrt{2}$, although our measurement of the magnetic populations cannot directly distinguish this delocalized state from an incoherent superposition of left- and right-localized states. Evidence of coherent dynamics is provided by the observation of oscillation, which occurs at roughly the expected period. Also shown are calculations of the corresponding magnetic populations, based on the lattice bandstructure. Note that in both experiment and theory the magnetic population distribution shows a pronounced dip at $m = 0$, which is indicative of a tunnelling situation where the localized wavepackets have minimal probability amplitude within the barrier.

Photon scattering destroys coherence between the left/right-localized states, though at a somewhat reduced rate because the dimension of the physical system is less than the optical wavelength [45]. At the experimental parameters

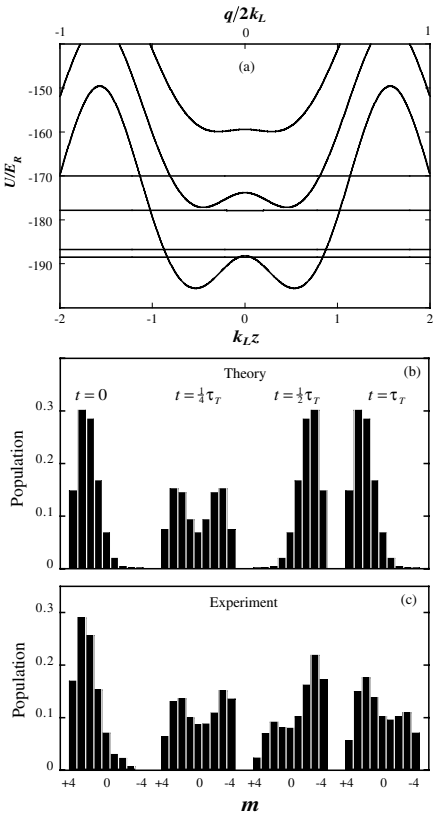

Figure 4. (a) Close-up of the lowest three adiabatic potentials and four exact energy bands of the magneto-optical lattice for the experimental parameters, $U_1 = 83E_{\mathrm{R}}$, $\theta = 80^\circ$, $B_x = 85$ mG and $B_z = 0$ mG. (b) Magnetic populations derived from the Bloch spinor states. (c) Experimentally measured magnetic populations. In both cases the system starts from a left-localized state at $t = 0$, and undergoes Rabi oscillations with a period $\tau_T \approx 275$ μs. Distributions are shown at four different times.

of figure 4 we estimate the photon scattering rate to be $\sim$600 s^{-1} for an atom localized near one of the double minima, when averaged over the relevant Clebsch–Gordan coefficients for the occupied magnetic sublevels. The atom, therefore, scatters a photon roughly once every six tunnelling periods, and we expect this to set the timescale for loss of coherence in the tunnelling oscillations. In practice an appreciable loss of contrast occurs after a single oscillation. We ascribe this to dephasing of the tunnelling oscillations, most likely due to inhomogeneity of the spurious effective B_z, as discussed above. We are hopeful that this and other sources of inhomogeneous broadening can be further suppressed or eliminated in future experiments. Moreover, our quasi two-level system should be amenable to the spin echo techniques that have been developed to solve essentially equivalent problems in nuclear magnetic resonance (NMR) spectroscopy.

4. Further developments

4.1. Reconstruction of the angular momentum density matrix

A major shortcoming of our current 'Zeeman microscope' is that the measured magnetic populations contain no direct

information about coherences in the double-well system. Information about internal state coherences between different m are of course available in the form of off-diagonal elements of the density matrix for the ground state angular momentum. For example, the delocalized states that occur during tunnelling oscillation can be directly distinguished from incoherent mixtures by the presence of large coherences between states m and $-m$. Clearly then, the systematic study of coherent dynamics and decoherence in our system will benefit greatly from extending our simple population measurement to a complete reconstruction of the angular momentum density matrix. In a complementary approach, motional coherences can be measured directly by interference of the atomic deBroglie waves in the far field [46].

An experiment is now underway in our group to implement a reconstruction scheme originally proposed by Newton and Young [31], which relies on repeated Stern–Gerlach measurements with respect to many different quantization axes. These measurements can be performed in a very straightforward manner, by choosing different directions for an applied bias magnetic field to establish the quantization axis after atoms are released from the lattice. The reconstruction algorithm requires that one measures the $2F + 1$ populations for $4F + 1$ different directions of the quantization axis, characterized by polar angles θ and azimuthal angles φ, as illustrated in figure 5(*a*). If one chooses a common θ and $4F + 1$ evenly separated φ in the interval $[0, 2\pi]$ it is possible to derive analytical expressions for the $(2F + 1)^2$ elements of the density matrix in terms of the $(2F + 1)(4F + 1)$ measured populations [31]. In practice it is much easier to relate the measured populations to the unknown elements of the density matrix by means of a rectangular matrix whose elements are determined by the set of angles θ and φ, and then invert the problem numerically. This allows us to choose a less restrictive set of angles that are more suited to the experimental geometry at hand, while at the same time keeping the reconstruction scheme numerically robust. To illustrate that a reasonable degree of robustness can be accomplished, figures 5(*b*) and (*c*) show a simulation of the reconstruction of a coherent superposition state $(|m = 4\rangle + |m = -4\rangle)/\sqrt{2}$ in the $F = 4$ ground state manifold of Cs, with realistic errors in the angles and population measurements.

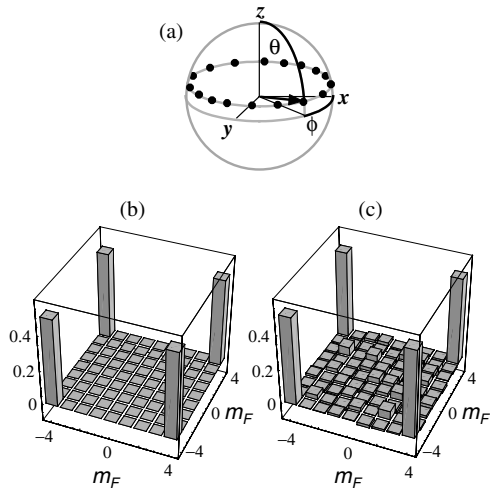

Figure 5. Reconstruction of the density matrix for an angular momentum. (*a*) The magnetic populations are measured repeatedly for $4F + 1$ different directions of the quantization axis (black dots), specified by a common polar angle θ and evenly separated azimuthal angles ϕ. (*b*) Density matrix for a state $(|m = 4\rangle + |m = -4\rangle)/\sqrt{2}$. (*c*) Simulated reconstruction of the density matrix for this state using $\theta = 83^\circ$, with 1° RMS errors on the angles θ and ϕ, and 5% RMS errors on the population measurements.

4.2. Classical versus quantum transport

When is the observed atomic transport to be interpreted as 'quantum tunnelling'? By tunnelling, we mean motion from one localized region to another which is forbidden by the classical equations of motion. For a scalar potential in one dimension, a bound state is uniquely defined as a tunnelling state if its total energy is less than the potential energy for some region between the classical outer turning points. For potentials with more than one degree of freedom, the identification becomes more ambiguous. In particular, for the magneto-optical lattice at hand, the potential energy depends not only on the position of the atom, but also on its internal state in a correlated way. If the BOA held, then one could recover an effectively scalar problem in which the dynamics are restricted to a single one-dimensional adiabatic potential. In contrast, because of the break down of the BOA, no single potential energy curve as a function of z uniquely defines the energy barrier presented to the atom in passing from one spin-polarized well to the other. In this situation, one cannot generally distinguish classically allowed from forbidden motion by analysis of the adiabatic potentials alone. An exception is when the energy is less than the barrier associated with the lowest adiabatic potential. In that case, classical motion is certainly forbidden as this adiabatic state represents the smallest possible potential energy in that region, and a total energy smaller than this is classically impossible. For energies above this adiabatic barrier, however, motion may *still* be classically forbidden, or highly unlikely, depending on the particular classical trajectory associated with the initial state. Furthermore, the initial conditions in this multidimensional problem are not uniquely defined by the total energy. Moreover, the coupling between the internal and external degrees of freedom leads to nonlinear equations of motion that can be classically chaotic, making the question of barrier traversal even more intriguing.

The distinction between classical and quantum barrier crossing for the multistate system has been studied by numerous authors in condensed matter [8] and chemical kinetics [1]. In most cases one assumes a system at thermal equilibrium and with substantial dissipation, in which case transport between the wells is overdamped. Transitions then occur as a rate phenomenon, rather than coherent oscillation. In the resulting model, known as 'transition rate theory' [1], the traversal rate is given by the rate of incidence of the particles on the barrier times the probability of traversing. In the context of the small polaron transport in the molecular-dimer approximation, Holstein calculated both the classical [47] and the quantum transition rate [48] assuming diabatic following, which he justified for this system.

Nonclassical motion then corresponds to energies below the crossing of the diabatic potentials. Wolynes has used the path integral influence functional method to characterize adiabatic versus nonadiabatic transitions in rate reactions [49]. Our system is essentially at zero temperature with minimal dissipation (in the ideal case). Tunnelling should thus proceed as a coherent oscillation rather than a decay process associated with incoherent hopping. Furthermore, as we will see below, for most parameter ranges neither the diabatic nor adiabatic approximation to the dynamics of the internal state is valid.

We turn then to a classical analysis of the dynamics. Given the form of the Hamiltonian associated with the magneto-optical potential far-off resonance, the problem corresponds to the motion of a massive particle with a magnetic moment moving in a combination of a scalar potential (independent of the moment) plus a spatially inhomogeneous magnetic field. The classical equations of motion then have the form

$$\dot{z} = p/m,$$
$$\dot{p} = -\frac{\mathrm{d}}{\mathrm{d}z}(U_0(z) - \vec{\mu}\cdot\boldsymbol{B}_{\mathrm{eff}}(z)), \tag{10}$$
$$\dot{\vec{\mu}} = \gamma(\vec{\mu}\times\boldsymbol{B}_{\mathrm{eff}}(z)),$$

where $\boldsymbol{B}_{\mathrm{eff}}(z) = B_{\mathrm{fict}}(z)\boldsymbol{e}_z + B_x\boldsymbol{e}_x$, with fictitious field as given in equation (4). These equation follow from the Heisenberg equations of motion, replacing the quantum operators by their expectation values and neglecting any correlations in the operator products.

Unlike the scalar case, specifying the energy does not uniquely constrain the trajectory. The magnitude of $\vec{\mu}$ is conserved, while its direction depends implicitly on time through the local magnetic field which varies both in magnitude and direction as the particle moves along the z-axis. This makes the effective phase space four dimensional (two external and two internal variables), which can be mapped onto a canonical pair of action-angle variables associated with two degrees of freedom [50]. In the harmonic approximation for $F = \frac{1}{2}$, this is essentially the Jaynes–Cummings problem of a coupled oscillator and spin, equation (7). With the rotating wave approximation we gain an additional conserved quantity, the total excitation, which together with conservation of energy makes the Hamiltonian integrable. The full Rabi Hamiltonian does not share this property, and the classical equations show deterministic chaos, as explored in the context of the atom–photon coupling [34] and the small polaron transport problem [50]. The optical lattice offers new opportunities to investigate the consequences of the classical chaotic dynamics in a regime that is deeply quantum.

One situation which allows an approximate separation of the Hamiltonian is the case of the BOA [51]. The potential energy can be expressed as a function of two variables, z and θ', the angle between the local magnetic field and the direction of the moment,

$$U_{\mathrm{ad}}(z,\theta') = U_0(z) - \mu B_{\mathrm{eff}}(z)\cos\theta'(z), \tag{11}$$

plotted in figure 6. The quantum mechanical adiabatic potentials associated with the extreme eigenvalues correspond to

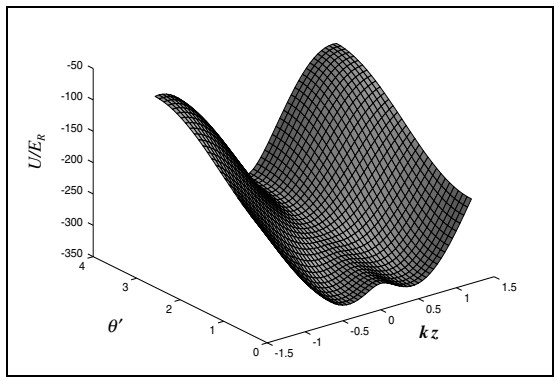

Figure 6. Adiabatic potential energy surface as a function of z and θ', the angle between the magnetic moment and the local direction of the effective magnetic field in the lin-θ-lin lattice with $U_1 = 150E_{\mathrm{R}}$, polarization angle $\theta = 68^\circ$ and transverse field $\hbar\gamma B_x = 33E_{\mathrm{R}}$. Adiabatic motion proceeds only along constant θ'. Along other directions the force must be supplemented by motional couplings.

$\cos\theta' = \pm 1$. Assuming adiabatic following of the moment, θ' becomes an additional constant of motion. Under this circumstance the energy barrier is well defined. Unfortunately, this approximation often breaks down in this system even for initial conditions on the adiabatic surface.

We numerically integrate equations (10) to obtain the classical trajectories associated with our optical lattice, with results shown in figure 7. We chose initial conditions with $p = 0$, and $\theta' = 0$; the initial position determines the total energy. For initial energy close to the bottom of the adiabatic double well, the magnetic moment remains aligned parallel to the magnetic field at all times. The external motion is regular and follows the adiabatic potential, remaining on the edge of the potential surface. For larger initial energies, the motion becomes nonadiabatic due to the large gradient of the magnetic field. The motion is highly stochastic, with long periods of localized oscillation, punctuated by random traversals between the two wells. A calculation of Lyaponov exponents shows the requisite exponential sensitivity to initial conditions. In addition, we plot the parameter $w = \cos\theta$, where θ is the true angle between the moment and the local field (adiabatic following corresponds to $w = 1$).

This has important implications for a deeper understanding of atomic transport in our system. Clearly, for energies E such that $E < U_{\mathrm{ad}}(z = 0, \theta' = 0)$, classical motion from one spin polarized well to the other is forbidden regardless of its path in spin-space. However, for energies above this barrier, when the particle does not follow the line $\theta' =$ constant, the classical dynamics may still trap the particle in one well over a substantial timescale. Experimental observation of magnetization oscillation between the spin-polarized states over a much shorter timescale would then correspond to quantum tunnelling. We are currently pursuing a systematic analysis of the predictions of classical dynamics for the parameter regime associated with the experiment presented in section 3.

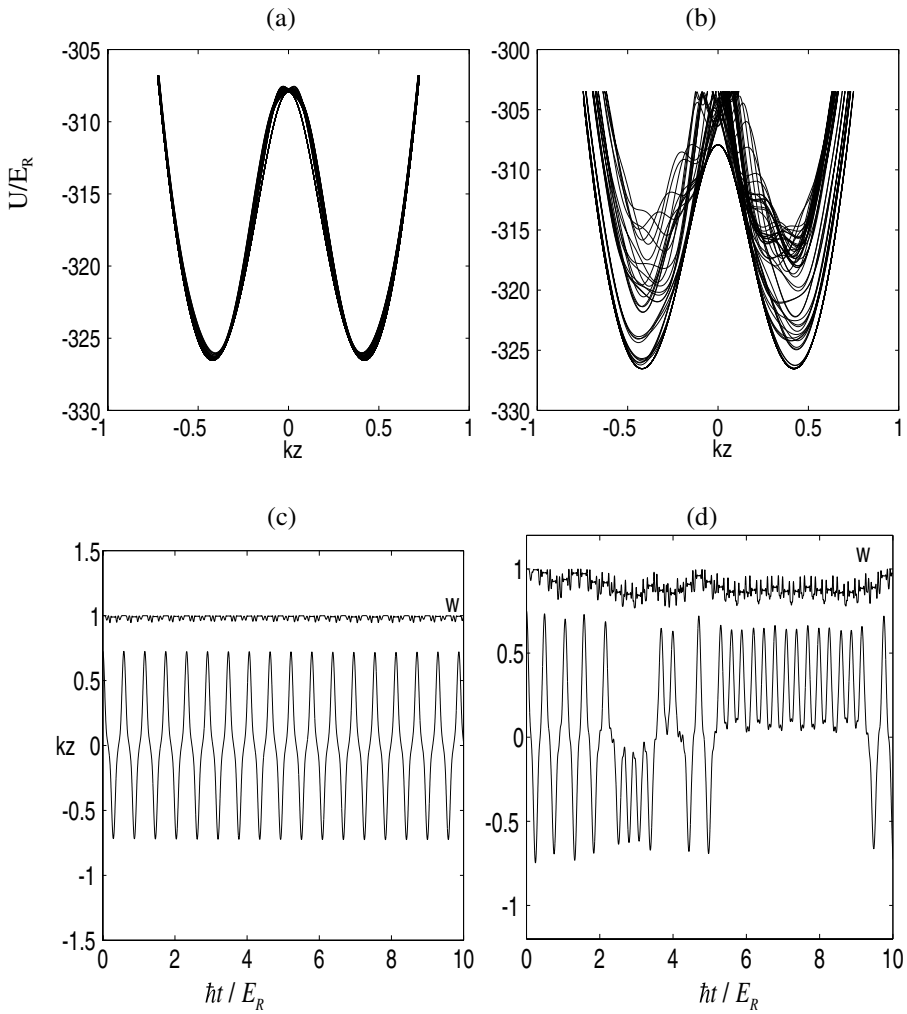

Figure 7. Numerical solutions to the classical equations of motion in the lin-θ-lin lattice, with parameters given in figure 6. Initial conditions are chosen with zero momentum and internal state in the adiabatic direction, $\theta' = 0$. The height of the adiabatic barrier is at $-308E_{\mathrm{R}}$. The initial position is set by the choice of total initial energy. The total potential energy is shown as a function of the trajectory along z for adiabatic following (*a*) with initial energy $-307E_{\mathrm{R}}$ and at a higher initial energy (*b*) $-303E_{\mathrm{R}}$, where the spin dynamics are not adiabatic. The corresponding position as a function of time is plotted in (*c*) and (*d*) respectively, together with the adiabatic parameter $w = \cos\theta'$. The nonadiabatic motion is chaotic.

5. Summary

We have presented here a means of exploring the rich variety of phenomena associated with the dynamics of a double-potential well in a controllable physical system—ultra-cold atoms moving in a magneto-optical lattice. Atoms trapped in oppositely polarized wells are coupled with a transverse magnetic field. Because of the correlation between the atomic position and internal state, precession of the atomic spin is accompanied by motion of the centre-of-mass wavepacket. Under appropriate conditions the atom can tunnel through the classically forbidden energy barrier. The entanglement between atomic spin and centre-of-mass motion provides a meter through which dynamical tunnelling and other transport phenomena can be directly observed at the microscopic level.

Coherent control of both internal and external degrees of freedom can be achieved in a manner that bears close resemblance to well-developed techniques in NMR. This analogy is made strong through the effective magnetic field picture of the optical potential, valid for alkali atoms with laser detuning large compared with the excited state hyperfine splitting. We model this control through numerical analysis of the bandstructure and solutions to the time-dependent Schrödinger equation for the ground-electronic hyperfine spinor. These simulations demonstrate the ability to perform quantum state preparation and control, and show strong magnetization oscillations which accompany quantum tunnelling.

Laboratory experiments employ caesium atoms in a one-dimensional, far-off resonance, magneto-optical lattice. Preparation of atoms in localized, pure quantum states in the double-potential wells is achieved through a combination of laser cooling, optical pumping and state selection. We use the entanglement between internal and external degrees of freedom to provide a meter for tunnelling dynamics. Measurement of the atomic spin is achieved through a 'Zeeman microscope', a variant of time-of-flight spectroscopy which allows separation of the narrow momentum distributions associated with the $2F + 1$

magnetic sublevels. This procedure can be extended to a complete reconstruction of the spin density matrix through a series of measurements along different quantization axes, thereby providing a diagnostic tool for analysing quantum coherences. Our experimental data clearly exhibits damped Rabi oscillations between mesoscopically distinct states, and demonstrates the potential for systematic study of coherent tunnelling dynamics. The main source of decoherence is photon scattering, which is modest compared with the Rabi frequency and too slow to explain the observed damping. Additional dephasing of the oscillations occur due to inhomogeneous broadening of the tunnelling resonance, which is caused by variation in lattice depth, polarization (fictitious magnetic field) and/or real magnetic field. Spin-echo techniques should allow us to extract the quantum coherent behaviour from this signal.

The entanglement between internal and external degrees of freedom makes our system a fertile arena for exploring complex dynamics. Whereas the definition of tunnelling in one dimension by a scalar particle in a static potential is precisely defined, for a vector particle the distinction between classical transport and quantum barrier penetration becomes ambiguous. Due to the extra degrees of freedom, the classical dynamics associated with our system takes place in a higher dimensional phase space which exhibits deterministic chaos when the spin does not adiabatically follow the direction of the local effective magnetic field. In the harmonic approximation this system is equivalent to the classical dynamics of the well-known spin–boson problem. Under such circumstances one must develop new criteria to distinguish classical barrier hopping from quantum tunnelling.

The manifestations of chaos in quantum mechanics and the emergent complexity at the classical level continues to be a problem of fundamental interest. Signatures of chaos at the classical level which appear in the quantum system have been explored in the spin–boson problem by many authors. Examples include the statistical properties of the eigenvalue spectrum (e.g. nonPoissonian spacing between nearest-neighbour energy levels) [52] and 'scars' in the quasiprobabilty distribution [53]. Though these are signatures of chaos, such analyses do not give a method to recover the full classical limit. Recently a new approach has shown that the classical chaos emerges when one includes a continuous measurement which only weakly perturbs the system and localizes the trajectories in phase space, consistent with the uncertainty principle [54]. In the limit $\hbar \to 0$ the classical Lyapunov exponents are recovered on these coarse grained trajectories [55]. The magneto-optical double-potential well thus provides a paradigm to explore nonlinear dynamics and the quantum–classical transition in a system which holds promise of well-controlled laboratory experiments.

Further studies will include the addition of a coherent drive to our system. Dynamic localization follows when the ratio of the driving amplitude to frequency satisfies a well-known resonance condition. The magneto-optic lattice should allow us to explore this phenomenon over a wide range of parameters, as we have shown in numerical simulations. The essence of this effect is contained in the dynamics of a driven two-level system when the population is maintained in the ground-band doublet. We can thus turn to the Bloch sphere picture of spin dynamics to gain a more intuitive understanding. Of particular interest is the effect of noise on this system. It has been shown under certain conditions that noise can stabilize the localization [15]. We are exploring this phenomenon in the context of both two-level dynamics as well as the full, multilevel description of our physical system.

Acknowledgments

We gratefully acknowledge helpful discussions with Gavin Brennen, Salman Habib, Tanmoy Bhattacharya, and Kurt Jacobs. IHD acknowledges support from the National Science Foundation (grant No PHY-9732456). PSJ was supported by the NSF (grant No PHY-9732612), by the Army Research Office (grant No DAAG559710165), and by the Joint Services Optics Program (grant No DAAG559710116).

References

[1] For reviews see Hänggi P, Talkner P and Borkovec 1990 *Rev. Mod. Phys.* **62** 251
[2] Ferry D K K and Jacoboni C (ed) 1992 *Quantum Transport in Semiconductors* (New York: Plenum)
[3] Kenkre V M 1982 *Exiton Dynamics in Molecular Crystals and Aggregates* ed G Höhler (Berlin: Springer)
Reineker P 1982 *Exiton Dynamics in Molecular Crystals and Aggregates* ed G Höhler (Berlin: Springer)
[4] Würger A 1997 *From Coherent Tunnelling to Relaxation* (Berlin: Springer)
[5] Caldeira A O and Leggett A J 1981 *Phys. Rev. Lett.* **46** 211
Caldeira A O and Leggett A J 1983 *Ann. Phys., NY* **149** 374
[6] Martinis J M, Devoret M H and Clarke J 1987 *Phys. Rev.* B **35** 4682
[7] Chudnovsky E M and Tejada J 1998 *Macroscopic Quantum Tunnelling of the Magnetic Moment* (Cambridge: Cambridge University Press)
[8] For a review, see Leggett A J *et al* 1995 *Rev. Mod. Phys.* **67** 725
[9] Weiss U 1993 *Quantum Dissipative Systems* (Singapore: World Scientific)
[10] Luis A A and Sethna J P 1995 *Phys. Rev. Lett.* **74** 1363
[11] Legett A J 1999 *J. Supercond.* **12** 683
[12] Giulin D *et al* 1996 *Decoherence and the Appearance of a Classical World in Quantum Theory* (Heidelberg: Springer)
[13] Lo H-K, Popescu S and Spiller T (ed) 1998 *Introduction to Quantum Computation and Information* (Singapore: World Scientific)
[14] Loss D and DiVincenzo D P 1998 *Phys. Rev.* A **57** 120
[15] For a review, see Grifoni M and Hänggi P 1998 *Phys. Rep.* **304** 230
[16] Dunlap D H and Kenkre V M 1986 *Phys. Rev.* B **34** 3625
Grossmann F *et al* 1993 *J. Stat. Phys.* **70** 229
[17] For a review, see Gammaitoni L, Hänggi P, Jung P and Marchesoni F 1998 *Rev. Mod. Phys.* **70** 223
[18] Ballentine L E and Lin W A 1990 *Phys. Rev. Lett.* **65** 2927
Ballentine L E and Lin W A 1992 *Phys. Rev.* A **45** 3637
Plata J and Gomez-Llorente J M 1992 *J. Phys. A: Math. Gen.* **25** L303
[19] Utermann R *et al* 1994 *Phys. Rev.* E **49** 273
Utermann R *et al* 1994 *Physica* B **194** 1013
[20] For a review, see Jessen P S and Deutsch I H 1996 *Adv. At. Mol. Opt. Phys.* **37** 95
[21] Ben Dahan M *et al* 1996 *Phys. Rev. Lett.* **76** 4508
[22] Wilkinson S R *et al* 1996 *Phys. Rev. Lett.* **76** 4512
[23] Niu Q *et al* 1996 *Phys. Rev. Lett.* **76** 4504

[24] Madison K W *et al* 1998 *Phys. Rev. Lett.* **81** 5093
[25] Dutta S K, Teo B K and Raithel G 1999 *Phys. Rev. Lett.* **83** 1934
[26] Hamann S E *et al* 1998 *Phys. Rev. Lett.* **80** 4149
[27] See special issue 1997 *J. Mod. Opt.* **44**
[28] Klappauf B G *et al* 1998 *Phys. Rev. Lett.* **81** 1203
[29] Deutsch I H and Jessen P S 1998 *Phys. Rev.* A **57** 1972
[30] Wineland D *et al* 1998 *Fortschr. Phys.* **46** 363
[31] Newton R G and Young B L 1968 *Ann. Phys., NY* **43** 393
[32] Jaynes E T and Cummings F W 1963 *Proc. IEEE* **51** 89
[33] Tavis M and Cummings F W 1968 *Phys. Rev.* **170** 379
[34] Belobrov I, Zaslavski G M and Tartalovski G Kh 1976 *Sov. Phys.–JETP* **44** 945
Milonni P W, Ackerhalt J R and Galbraith H W 1983 *Phys. Rev. Lett.* **50** 966
Milonni P W, Shih M-L and Ackerhalt J R 1987 *Chaos in Laser–Matter Interactions* (Singapore: World Scientific)
[35] Happer W and Mathur B S 1967 *Phys. Rev.* **163** 12
[36] Finkelstein V, Berman P R and Guo J 1992 *Phys. Rev.* A **45** 1829
[37] Deutsch I H, Grondalski J and Alsing P M 1997 *Phys. Rev.* A **56** R1705
[38] Garraway B M and Suominen K-A 1995 *Rep. Prog. Phys.* **58** 365
[39] Kosloff R 1988 *J. Phys. Chem.* **92** 2087
[40] Riley M E and Ritchie B 1999 *Phys. Rev.* A **59** 3544
[41] Vesely F J 1994 *Computational Physics: an Introduction* (New York: Plenum)
[42] Haycock D L *et al* 1998 *Phys. Rev.* A **57** R705
[43] Haycock D L *et al* 1997 *Phys. Rev.* A **55** R3991
[44] Goldner L S *et al* 1994 *Phys. Rev. Lett.* **72** 997
[45] Chapman M S *et al* 1995 *Phys. Rev. Lett.* **75** 3783
Cirac J I, Schenzle A and Zoller P 1994 *Europhys. Lett.* **27** 123
[46] Grondalski J, Alsing P M and Deutsch I H 1999 *Opt. Express* **5** 249
[47] Holstein T 1959 *Ann. Phys., NY* **8** 343
[48] Holstein T 1978 *Phil. Mag.* B **37** 49
[49] Wolynes P G 1987 *J. Chem. Phys.* **86** 1957
[50] Feinberg D and Ranninger J 1984 *Physica* D **14** 29
[51] Schanz H and Esser B 1997 *Phys. Rev.* A **55** 3375
[52] Graham R and Höhnerbach 1984 *Z. Phys.* B **57** 233
Graham R and Höhnerbach 1987 *Quantum Measurement and Chaos* ed E R Pike and S Sarkar (New York: Plenum)
Kús M 1985 *Phys. Rev. Lett.* **54** 1343
Lewenkoph C H *et al* 1991 *Phys. Lett.* A **155** 113
[53] Aguiar M A M *et al* 1991 *Europhys. Lett.* **15** 125
Leschke H, Nagel P, Muller L and Stolze J 1991 *Phys. Rev.* A **44** 1022
[54] Fukuo T, Ogawa T and Nakamura K 1998 *Phys. Rev.* A **58** 3293
[55] Bhattacharya T, Habib S and Jacobs K 1999 *Phys. Rev. Lett.* submitted
(Bhattacharya T, Habib S and Jacobs K 1999 *Preprint* LANL eprint quant-ph/9906092)